

# The morphodynamics of 3D migrating cancer cells

Christopher Z. Eddy,<sup>1</sup> Xinyao Wang,<sup>2</sup> Fuxin Li,<sup>2</sup> and Bo Sun<sup>1</sup>

<sup>1</sup>*Department of Physics, Oregon State University, Corvallis OR, 97331*

<sup>2</sup>*School of Electrical Engineering and Computer Science, Oregon State University, Corvallis OR, 97331*

Cell shape is an important biomarker that is directly linked to cell function. However, cell morphodynamics, namely the temporal fluctuation of cell shape is much less understood. We study the morphodynamics of MDA-MB-231 cells in type I collagen extracellular matrix (ECM). We find ECM mechanics, as tuned by collagen concentration, controls the morphodynamics but not the static cell morphology. We employ machine learning to classify cell shape into five different morphological phenotypes corresponding to different migration modes. As a result, cell morphodynamics is mapped into temporal evolution of morphological phenotypes. We systematically characterize the phenotype evolutions including occurrence probability, dwell time, transition flux, and 3D migrational characteristics. We find that manipulating Rho-signaling enhances the morphodynamics and phenotype transitions. Using a tumor organoid model, we show that the distinct invasion potentials of each phenotype modulate the phenotype homeostasis. Overall invasion of a tumor organoid is facilitated by individual cells searching for and committing to phenotypes of higher invasive potential. In conclusion, we show that 3D migrating cancer cells exhibit rich morphodynamics that is regulated by ECM mechanics, Rho-signaling, and is closely related with cell motility. Our results pave the way to the systematic characterization and functional understanding of cell morphodynamics as a new biomarker for normal and malignant cells.

## INTRODUCTION

Shape defines the cell. In the 1677 book *Micrographia*, Robert Hooke showed sections within a herbaceous plant under a microscope. The shape of those sections resembles cells in a monastery, so he named the structures cells [1]. Many breakthroughs followed Hooke's discovery, from the cell theory of Schwann and Schleiden, to the theory of tissue formation by Remak, Virchow and Kolliker, and the theory of cellularpathologie by Virchow, all of which are inspired by observations of cell shapes, or morphology in general [2, 3].

In our modern view cell shape is determined by cell function [4, 5]. A nerve cell has long branched protrusions for communication with other neurons; while the cuboidal shape of epithelial cells allow them to tile the surface of organs. Loss of characteristic shape, on the other hand, is associated with functional abnormality. Thus morphological characterization has been an important tool for diagnosis such as in red blood cell disease [6], neurological disease [7], and cancer [8, 9]. More recently, cell shape analysis is boosted by techniques from computer vision. As a result, it becomes possible to obtain high content information of cellular states from morphological data alone [9–12].

While most research focuses on the static cell morphology, the dynamic fluctuation of cell shape is much less understood. However, shape fluctuation – namely morphodynamics, is of central importance for dynamic cellular functions. The abnormal diffusion of small protrusions - microvilli - on the surface of a T cell allows the T cell to efficiently scan antigen-presenting surfaces [13]. For a migrating cancer cell, morphodynamics drives the motility of the cell in many ways similar to our body frame

movements that enable swimming. In fact, just as there are different swimming styles, cancer cells have been observed to execute six different programs during invasion in 3D tissue space [14]. Each program has distinct signatures of morphology and morphodynamics, and are usually referred to as migration phenotypes of filopodial, lamellipodial, lobopodial, hemispherical blebbing, small blebbing, and actin-enriched leading edge [15]. Cancer cell migration phenotypes are controlled by intracellular signaling such as the Rac and Rho-Rock-myosin pathways [16, 17], and extracellular factors such as the elasticity, and degradability of the extracellular matrix (ECM) [18, 19]. The ability of a cancer cell to switch between migration phenotypes is important for tumor prognosis. Many therapies, such as MMP inhibitors that target a particular mode of cell motility, fail to stop tumor metastasis largely because cells take other available migration programs [20, 21].

In this paper, we study the morphodynamics of MDA-MB-231 cells, a highly invasive human breast cancer cell line in 3D collagen matrices. We find the shape fluctuation is regulated by the mechanics of ECM. The cellular morphodynamics not only drives 3D migration, but also allows a single cell to sample multiple morphological phenotypes over a short amount of time. As a result, ECM mechanics regulate the stability and transitions between morphological phenotypes that corresponding to different migration programs. We have measured the motility of each morphological phenotype and find that phenotype transition facilitates invasiveness during 3D tumor organoid invasion.

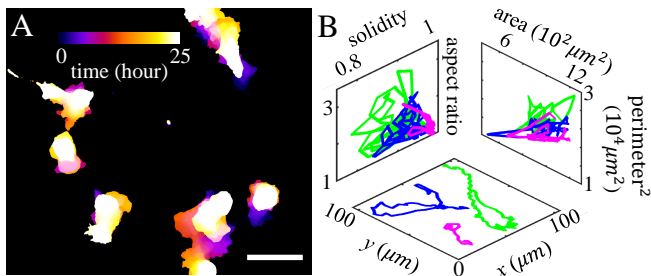


FIG. 1. Three-dimensional migration of MDA-MB-231 cells is accompanied with significant cell shape fluctuation. (A) A typical time lapse recording of 25 hours is projected onto a single image with colors representing time. (B) The real space (x-y plane), and shape space trajectories of 3 cells shown in (A).

## RESULTS

We find 3D migrating cancer cells rapidly sample their available shape space. In order to quantify the cell morphodynamics, we take time-lapse fluorescent images of MDA-MB-231 cells migrating in collagen matrices. The GFP labeled cells typically stay within the focal depth of the objective lens (20X, NA 0.7) for 10-20 hours, while we obtain 2D cell images at a rate of 4 frames per hour (see *SI Appendix* section S1). After binarization and segmentation, we compute geometric measures such as area, perimeter, aspect ratio, and solidity which collectively quantify the shape of a cell (see *SI Appendix* section S2).

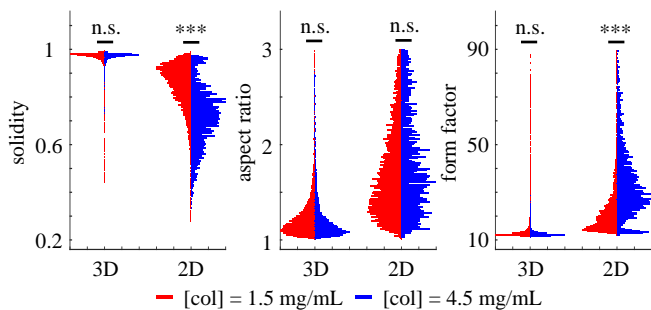


FIG. 2. Ensemble distribution of shape characteristics of MDA-MB-231 cells in 3D (embedded in collagen gels) and 2D (on the top surfaces of collagen gels) cultures. The histograms show relative probabilities (peak normalized to one) of solidity, aspect ratio, and form factor. For each distribution sample size  $N > 2000$ . \*\*\*:  $p < 0.001$ , n.s.: not significant (ANOVA). Color of the bars represent collagen concentration, red: 1.5 mg/mL, and blue: 4.5 mg/mL.

The morphodynamics of a cell manifests itself as a random walk in the geometric shape space concurrent with its motility in the 3D matrix (Fig. 1). Because any cell shape change boils down to the physical interactions between the cell and its environment, we hypothesize that morphodynamics is sensitive to the physical properties of

the ECM. To test the hypothesis, we examine the shape fluctuation of thousands of MDA-MB-231 cells in type I collagen matrices of varying concentrations (see *SI Appendix* section S2). As we increase collagen concentration from 1.5 mg/mL to 4.5 mg/mL, the storage modulus increases by more than three folds (see *SI Appendix* section S3).

We first examine if ensemble distributions of cell shape shift as collagen concentration increases. To this end we focus on three quantifies: solidity (ratio of the area and its convex area), aspect ratio (ratio of the major and minor axes lengths), and form factor (ratio of squared perimeter and area) that are independent of imaging scales. As shown in Fig. 2, these quantities are sharply distributed for 3D migrating cells. However, none of the three quantities show significant changes when collagen concentration increases by 3-fold. This is in clear contrast to MDA-MB-231 cells migrating on 2D surfaces. Consistent with previous reports, when collagen concentration increases from 1.5 mg/mL to 4.5 mg/mL, MDA-MB-231 cells exhibit lower solidity and higher form factor, as a result of enhanced integrin-mediated adhesion and membrane protrusions [22].

While the ensemble distributions of cell shape do not distinguish between different collagen concentrations in 3D cultures, we find morphodynamics do. For 3D migrating cells we calculate their mean square displacements in real space ( $\sigma_{xy}^2$  in Fig. 3A) and in shape space ( $\sigma_{sol}^2$ ,  $\sigma_{asp}^2$ , and  $\sigma_{for}^2$  in Fig. 3B-D). MDA-MB-231 cells show higher diffusivity in real space at lower collagen concentration, as is expected when matrix pore size is rate-limiting for cell migration [23, 24].

Remarkably, cellular morphodynamics show clear dependence on collagen concentrations. Over the time scale of a few hours,  $\sigma_{sol}^2$ ,  $\sigma_{asp}^2$ , and  $\sigma_{for}^2$  are approximately linear functions of time. Interestingly, diffusivity of solidity, aspect ratio, and form factor are highest at intermediate collagen concentration (3.0 mg/mL), and are strongly suppressed at collagen concentration of 4.5 mg/mL.

The fact that ECM mechanics significantly regulates cellular morphodynamics, but not static cell shapes, may be understood from a simple physical picture. The morphodynamics of a cell may be considered as a random walk over a complex potential landscape  $\mathcal{U}_{shape}$  defined over the cell shape space. At equilibrium, the distribution of static cell shape (Fig. 2) is determined by  $\mathcal{U}_{shape}$  while the speed of fluctuation (Fig. 3) is also influenced by the effective viscosity. Keeping this simple picture in mind, we conclude that for 2D migration ECM concentration regulates the topography of the potential landscape while in 3D ECM concentration mainly affects the effective viscosity.

Motivated by the mechanosensitivity of cell shape fluctuation, we next seek to gain more insights by investigating a course-grained version of morphodynamics. To this end, we train machine classifiers to divide the high dimen-

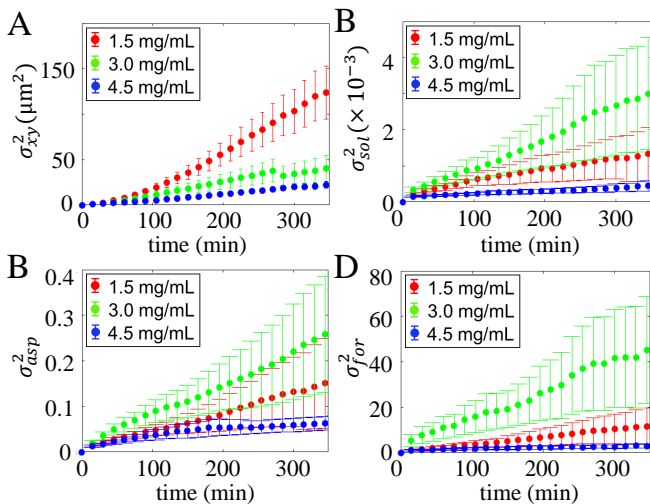


FIG. 3. The mean square displacement (MSD)  $\sigma^2$  of MDA-MB-231 cells in real space and in shape space as a function of time  $t$ . (A) MSD of real space motility.  $\sigma_{xy}^2$  is obtained from the x-y components of 3D cell trajectories. (B-D) MSDs characterize the fluctuation of solidity ( $\sigma_{sol}^2$ ), aspect ratio ( $\sigma_{asp}^2$ ), and form factor ( $\sigma_{for}^2$ ). For each collagen concentration about 200 cells are analyzed.

sional cell shape space based on 3D cell migration phenotypes. This is possible because different migration modes are associated with distinct characteristic cell morphologies [14, 19].

We consider five morphological phenotypes including two mesenchymal ones: filopodial (or FP in short) and lamellipodial (LP); as well as three amoeboidal ones: hemispherical blebbing (HS), small blebbing (SB), and actin-enriched leading edge (AE). A sixth phenotype, namely lobopodial or nuclear piston mode, has not been observed in our experiments which is consistent with previous reports [25]. Once the classifier is trained, phenotype is determined automatically from a cell image if a particular phenotype receives more than 70% probability score. On the other hand, if none of the five phenotypes receive more than 70% probability score, the cell is considered to be in an intermediate state.

We have trained two classifiers (see *SI Appendix S4*). The first one is based on support vector machines (SVM [26, 27]) involving 66 geometric measures. The second one is based on a convolutional neural network architecture that uses raw gray scale images as inputs [28]. Both classifiers show good separation of training sets, more than 90% of successful rates, and agree with each other well on test data sets (Fig. 4A and *SI Appendix S4*). Following, we mainly report the results from SVM algorithm since it has intuitive interpretations directly from the geometric measures.

The likelihoods of observing different morphological phenotypes are remarkably different. At  $[\text{col}] = 1.5$  mg/mL, HB, LP and SB shapes each account for more

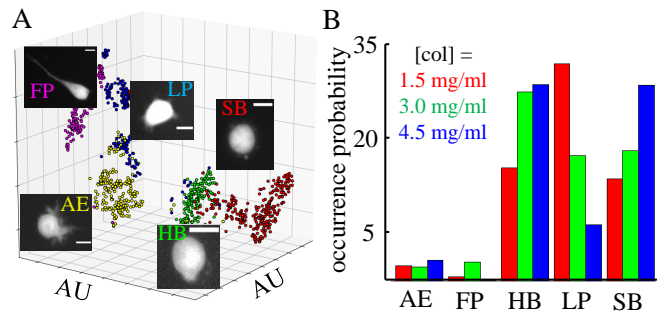


FIG. 4. MDA-MB-231 cells exhibit multiple morphological phenotypes that are typically associated with distinct 3D migration modes. (A) An SVM classifier is trained based on geometry of binarized cell images. A threshold of 70% probability is required for each phenotype classification, or the cell is classified to be in intermediate state. To better visualize the high dimensional geometric measures, we apply t-SNE method [29] to generate a 3D projection of the cell shape spaces. Different morphological phenotypes (insets show representative images) are clearly separated. Scale bars of the insets are  $20 \mu\text{m}$ . (B) Percentage occurrence of each morphological phenotype (intermediate states account for approximately 30% occurrence in each collagen concentration). AE: actin-enriched leading edge. FP: filopodial, LP: lamellipodial, HS: hemispherical blebbing, SB: small blebbing. Colors represent collagen concentration, red: 1.5 mg/mL, green: 3 mg/mL, blue: 4.5 mg/mL. For each collagen concentration more than 3000 single cell images are analyzed.

than 15% of the observations, FP and AE phenotypes only occur less than 5% of the time. We find increasing collagen concentration increases the occurrence of HS and SB cells, while decreasing the occurrence of LP cells. This observation suggests that phenotype homeostasis of MDA-MB-231 cells is regulated by ECM mechanics such that stiffer ECM promotes higher probability of amoeboidal phenotypes.

To obtain further insights of cell morphodynamics, we investigate the time evolution of morphological phenotypes. Fig. 5A shows a typical time series of phenotype dynamics where a cell switch directly from FP to LP shape, then to SB shape via intermediate state. We first examine the overall stability of cell shapes by measuring the average dwell time a cell staying continuously either in amoeboidal or mesenchymal states (see also *SI Appendix S5*). As shown in Fig. 5B, amoeboidal dwell time  $T_d^a$  slightly increases with collagen concentration, while mesenchymal dwell time  $T_d^m$  decreases. At concentration  $[\text{col}] = 1.5$  mg/mL,  $T_d^a = 3.8$  hrs is more than twice longer than  $T_d^m = 1.6$  hrs. When collagen concentration increases to 4.5 mg/mL, mesenchymal shapes become less stable, and the corresponding dwell time (2.4 hrs) is only 30% longer than the amoeboidal dwell time (1.8 hrs).

To reveal the details of phenotype dynamics, we have computed the transition rates as shown in Fig. 5C-D. Surprisingly, we notice that while higher ECM concentration extends the amoeboidal dwell time, it doesn't

slow down the phenotype dynamics at all. Instead, we observe more frequent transitions along the HB-SB-AE amoeboidal axes. For instance, the transition rates between HB and SB states at  $[col] = 4.5$  mg/mL is 20% higher than the rates at  $[col] = 1.5$  mg/mL. While on the contrary, the transition rates along the mesenchymal axis FP-LP barely change when collagen concentration increases by 3 folds.

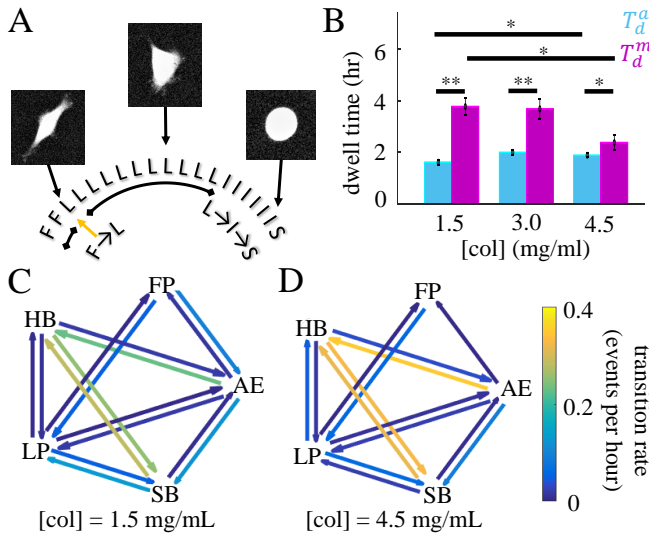


FIG. 5. Collagen concentration regulates the morphological phenotype homeostasis of 3D migrating MDA-MB-231 cells. (A) A sample time series of morphological phenotype. Insets: three snapshots showing the GFP-labeled cell. Abbreviations: F – filopodial, L – lamellipodial, I – intermediate state. (B) The dwell times of amoeboidal ( $T_d^a$ , cyan) and mesenchymal ( $T_d^m$ , magenta) cell shapes have opposite dependence on collagen concentration. (C-D) Graphical representation of the transition matrix between different morphological phenotypes at collagen concentration of 1.5 mg/mL (c) and 4.5 mg/ml (D). The results of (B-D) are obtained by analyzing a total of more than 6200 hours (four frames per hour) of single cell morphodynamic trajectories. See also *SI Appendix S5* for additional details.

Results in Fig. 5C-D also reveal that the reduction of mesenchymal dwell time  $T_d^m$  at higher collagen concentration is mainly due to the two-fold increase of transition rates from lamellipodial to amoeboidal states. This is consistent with the mechanical model of blebbing formation [30, 31]. A lamellipodial cell exhibits a prominent cortical F-actin layer. Blebbs form when actomyosin contractility exceeds the binding between cortical actin and cell membrane. Our results suggest that the two competing forces exhibit higher fluctuation at increased ECM concentration, fueling the transition between lamellipodial and blebbing states.

On the other hand, we observe that filopodial cells have very low transition rates to and from blebbing phenotypes. Filopodial protrusions consist of elongated and bundled actin fibers as a result of elevated actin poly-

merization and cross-linking by Ena/VASP proteins [32]. Fig. 5C-D suggest that the mechanical barrier separating filopodia and blebbing protrusions is too high for the actomyosin contractility to overcome directly. Instead, a FP cell can turn into a blebbing shape by first transform into AE or LP states.

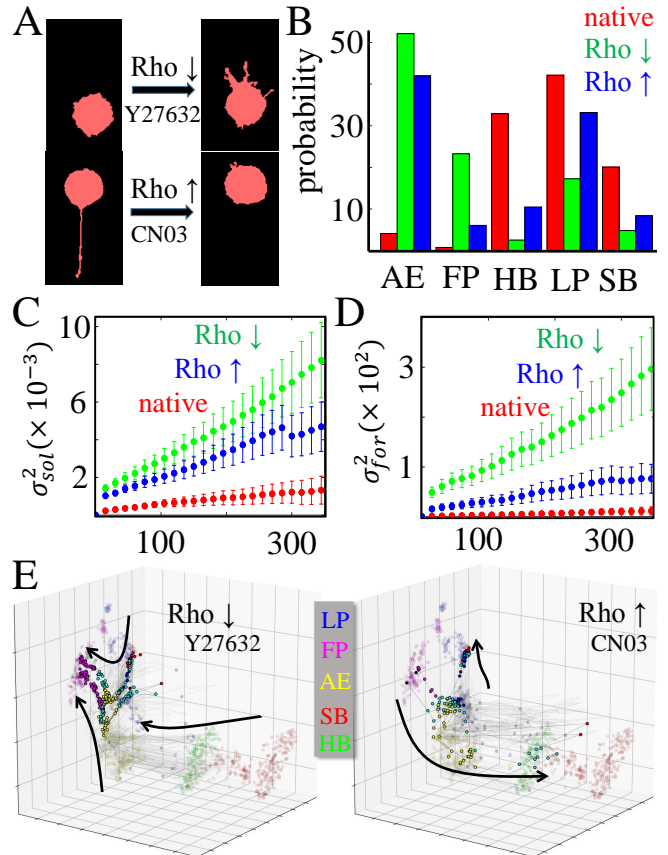


FIG. 6. Morphodynamics of 3D cultured MDA-MB-231 cells under pharmacological perturbations of Rho-signaling. (A) Representative morphological changes under treatment of Y27632 or CN03. (B) The occurrence probabilities of each morphological phenotypes after 8 hours of Y27632 (Rho $\downarrow$ ) and CN03 (Rho $\uparrow$ ) treatments. (C-D) The mean square displacement  $\sigma^2$  of solidity ( $\sigma_{sol}^2$ ) and form factor ( $\sigma_{for}^2$ ) for native (nontreated), Y27632-treated, and CN03-treated cells. (E) Trajectories (thin gray lines) of cells in the t-SNE embedded shape space. The trajectories start immediately after introducing Y27632 or CN03, and ends after 8 hours of incubating with the drugs. Converging paths are indicated with thick curves with arrows as guide to the eyes. Two representative trajectories per each treatment are highlighted with colored dots connected by black lines, where color represents the instantaneous phenotype. Scattered light-colored dots show training sets which is the same as in Fig. 4A. For each treatment approximately 100 cells are analyzed for their morphodynamics.

In order to understand the mechanisms underlying cell morphological phenotype transitions, we examine the effects of manipulating Rho-signaling, which is a master regulator that determines the mechanical state of a cell.

To this end, we apply Y27632, a Rho-inhibitor; and CN03, a Rho-activator to MDA-MB-231 cells cultured in collagen ECM with concentration of 1.5 mg/mL (see *SI Appendix S1*). Consistent with previous reports, Y27632 reduces actomyosin contractility, promoting transitions from blebbing to mesenchymal phenotypes [22]. On the other hand, CN03 elevates myosin II activity, leading to retraction of filopodia to rounded cell shapes (Fig. 6A). We find that after the treatment, occurrence probabilities of morphological phenotypes are markedly distinct from the native (non-treated) cells (Fig. 6B). Perturbing the Rho signaling in both directions encourage the cells to sample their shape space more dynamically (Fig. 6C-D). As a result, both Y27632 and CN03 treatments allow the cells to more frequently visit otherwise hard to access states such as FP and AE. Invigorated by the perturbations, MDA-MB-231 cells exhibit reduced disparity in the phenotype occurrence probabilities compared with the native (non-treated) group.

Tracking the phenotype evolution at single cell resolution further reveals the shape trajectories of MDA-MB-231 cells under perturbations (Fig. 6E). Despite fluctuations among individual cells, we find strong convergence of trajectories in cell shape space (Fig. 6E thick arrows). These converged paths are presumably the most biomechanically favorable. Consistent with our results in Fig. 5, AE state is heavily accessed as a gateway to FP state when cells are treated with Y27632. When treated with CN03, AE is at the fork of two bifurcating directions where one lead to LP, and the other lead to HB/SB states. These results suggest that AE state, which exhibits weak cell-ECM adhesions and F-actin rich protrusions [33, 34], mediate Rho-signaling controlled transitions between mesenchymal and amoeboidal motility.

Having analyzed the morphodynamics of MDA-MB-231 cells in 3D matrices, we next examine the invasion potential of each morphological phenotype. To this end, we model the migration of a cell as a polarized persistent random walk [35]. Because the finite dwell time of each phenotype limits the length of trajectories, we measure step size distribution as an alternative of autocorrelation analysis in order to extract the diffusivity and persistence of cell motility for each phenotype.

We consider one-hour segments of cell trajectories divided into two half-hour sections. Assuming the average cell velocity during the first section is along  $\hat{x}$  direction, we find the displacement  $\delta\mathbf{d}$  of the cell in the second section well described as

$$\begin{aligned}\delta\mathbf{d} &= d_{\parallel}\hat{x} + d_{\perp}\hat{y} \\ &= W(v_{\parallel}\delta t, D_{\parallel}\delta t)\hat{x} + W(0, D_{\perp}\delta t)\hat{y},\end{aligned}\quad (1)$$

where  $\delta t = 0.5$  hour,  $W(\mu, \sigma^2)$  is a Wiener process of drift  $\mu$  and variance  $\sigma^2$  (See also *SI Appendix S6*).  $D_{\parallel}$  and  $D_{\perp}$  are effective diffusion coefficients of the cell in two orthogonal directions: one that is parallel to the previous step, and one that is perpendicular to the previous

step.  $v_{\parallel}$  is the persistent velocity, which quantifies the tendency of a cell to keep its migration direction.

We find overall filopodial cells have the highest rate of persist migration (Fig. 7A-B and *SI Appendix S6*), while SB mode is the least motile. The phenotype-dependent motility is also tuned by the ECM mechanics. In particular,  $v_{\parallel}$  and  $D_{\parallel}$  are maximal at intermediate collagen concentration for mesenchymal modes (3 mg/ml), but the trend is not present for amoeboidal modes. Previously it was reported that MDA-MB-231 cell invasion is most efficient at intermediate collagen concentration [36]. Here we show that mesenchymal motility is mostly responsible for such non-monotonic dependence.

Persistent motility predicts the invasion potential of cancer cells. Because of the observed phenotype transitions (Fig. 5), we expect that phenotype homeostasis is coupled with invasion. In particular, we hypothesize a population selected for higher invasion potential will have different phenotype occurrence probability compared with the random migration assays in Fig. 4.

To test the hypothesis, we study the invasion of a tumor diskoid into ECM of 1.5 mg/ml type I collagen [37]. The diskoid of 500  $\mu\text{m}$  in diameter consists of  $\approx 1500$  tightly packed MDA-MB-231 cells. Over the course of 5 days, cells disseminate into the ECM as deep as 400  $\mu\text{m}$  from the original tumor. Fig. 7C shows a snapshot taken on the fifth day of the invading diskoid (See also *SI Appendix S7*).

We examine the morphological phenotype of all cells that have disseminated from the original tumor. Consistent with our hypothesis, this more invasive population favors AE and FP modes, which have the highest persistent motility at  $[\text{col}]=1.5$  mg/ml as shown in Fig. 7A-B. On the other hand, the slow moving SB modes only account for 8% of the population disseminated from the original tumor organoid. The shift of phenotype homeostasis is especially striking when comparing Fig. 4B and Fig. 6C, where the most and least probable phenotypes are opposite in these two situations.

## DISCUSSION

In this paper, we report the morphodynamics of MDA-MB-231 cells in type I collagen ECM as a model system of metastatic cancer cells migrating in 3D tissue. MDA-MB-231 cells rapidly sample their possible geometry, therefore exhibiting simultaneous random walks in both real space and shape space (Fig. 1). When ECM mechanics are tuned by varying collagen concentration, we find dramatic changes in the cellular morphodynamics, but not in the ensemble distributions of cell shapes (Fig. 2 and Fig. 3). On the other hand, when the cells migrate on the surfaces of collagen ECM, their shape distributions do shift as collagen concentration increases. The contrast is particularly striking noticing that almost

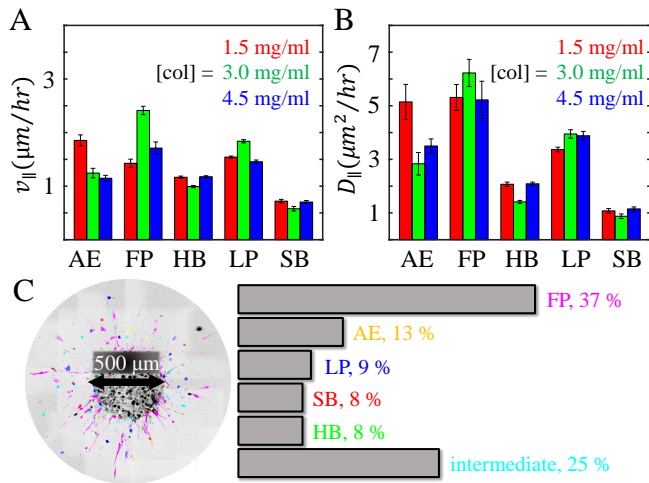


FIG. 7. The morphological phenotype determines 3D invasive potential of MDA-MB-231 cells. (A-B) Persistence and diffusivity of each morphological phenotype in ECM of varying collagen concentrations. For each condition,  $v_{\parallel}$  and  $D_{\parallel}$  are obtained by fitting the cumulative distribution function of samples with  $N > 1000$ . The errorbars are 95% confidence intervals of the fitting parameters. See also *SI Appendix S6* for more details. (C) Phenotype composition of cells disseminated from the original tumor organoid at day 5 after seeding the cells. Left: a confocal imaging snapshot of an organoid taken at day 5. Cells that have disseminated into the ECM are color-labeled by their phenotype classification. Right: phenotype composition of disseminating cells.

the same set of molecular machineries are involved in both 2D and 3D cell migration, shape regulation and mechanosensing [38, 39].

The biological significance of the morphodynamics is further demonstrated by classifying cell shapes into morphological phenotypes corresponding to different migration programs. While the occurrence and dwell time of blebbing phenotypes increases with collagen concentration, mesenchymal shapes become less stable and probable (Fig. 4 and Fig. 5). Interestingly, accompanying these two opposite trends is the increased transition rates among morphological phenotypes that are elevated at higher collagen concentration (Fig. 5).

Our results also shed light to the control mechanism of cell motility phenotypes. In particular, we show that perturbing the Rho-signaling dramatically modulates the cell morphodynamics (Fig. 6). It has been shown previously that Rac and Rho signaling regulates the shift between lamellipodial and blebbing motility [16, 18]. Complement to these results, our analysis further reveal that instead of stabilizing a particular mode of motility, perturbation of Rho signaling invigorates the morphodynamics of cells. As a result, cells exhibit more dynamic shape fluctuations and more aggressively explore the different morphological phenotypes. We also find that AE state mediate the Rho-signaling controlled transitions be-

tween different phenotypes, further illuminating the underlying phenotype landscape that controls cancer cell 3D motility.

In light of the rapid phenotype transitions exhibited by individual cells, 3D cancer cell motility may be considered as a hidden Markov process where each phenotype is associated with characteristic diffusivity and persistence. In this perspective morphodynamics facilitates cancer invasion because phenotype transitions allow cancer cells to search for and commit to a more invasive phenotype (Fig. 7), [40].

In summary, we demonstrate the morphodynamics of 3D migrating cancer cells as a powerful tool to inspect the internal state and microenvironment of the cells. In order to further exploit the information provided by the cell shape fluctuations, future research is needed to decode morphodynamics as a rich body language of cells, and to control morphodynamics as a route of mechanical programming of cell phenotype.

## MATERIALS AND METHODS

See *SI Appendix S1* for details of 3D cell culture, microscopy, and pharmacological treatments.

We thank Prof. Michelle Digman and Prof. Steve Pressé for helpful discussions. The funding for this research results from a Scialog Program sponsored jointly by Research Corporation for Science Advancement and the Gordon and Betty Moore Foundation through a grant to Oregon State University by the Gordon and Betty Moore Foundation

- 
- [1] R. Hooke, *Micrographia* (The Royal Society, 1665).
  - [2] P. Mazzeo, *Nat. cell biol.*, E13 (1999).
  - [3] E. Mayr, *The Growth of the Biological Thought* (Belknap, Cambridge, MA, 1982).
  - [4] B. Alberts, A. Johnson, J. Lewis, D. Morgan, M. Raff, K. Roberts, and P. Walter, *Molecular biology of the cell* (Garland Science, 2014).
  - [5] R. Singhvi, A. Kumar, G. P. Lopez, G. N. Stephanopoulos, D. I. Wang, G. M. Whitesides, and D. E. Ingber, *Science* **264**, 696 (1994).
  - [6] M. Diez-Silva, M. Dao, J. Han, C.-T. Lim, and S. Suresh, *MRS bulletin / Materials Research Society* **35**, 382 (2010).
  - [7] A. Serrano-Pozo, M. P. Frosch, E. Masliah, and B. T. Hyman, *Cold Spring Harbor Perspectives in Medicine* **1**, a006189 (2011).
  - [8] Z. Yin, A. Sadok, H. Sailem, A. McCarthy, X. Xia, F. Li, M. A. Garcia, L. Evans, A. R. Barr, N. Perrimon, C. J. Marshall, S. T. C. Wong, and C. Bakal, *Nat. Cell Biol.* **15**, 860 (2013).
  - [9] P.-H. Wu, J. M. Phillip, S. B. Khatau, W.-C. Chen, J. Stirman, S. Rosseel, K. Tschudi, J. Van Patten,

- M. Wong, S. Gupta, A. S. Baras, J. T. Leek, A. Maitra, and D. Wirtz, *Sci. Rep.* **5** (2015), 10.1038/srep18437.
- [10] C. Bakal, J. Aach, G. Church, and N. Perrimon, *Science* **316**, 1753 (2007).
- [11] V. K. Lam, T. C. Nguyen, B. M. Chung, G. Nehmetallah, and C. B. Raub, *Cytometry Part A* **93**, 334 (2017).
- [12] J. C. Caicedo<sup>1</sup>, S. Cooper, F. Heigwer, S. Warcha, P. Qiu, C. Molnar, A. S. Vasilevich, J. D. Barry, H. S. Bansal, O. Kraus, M. Wawer<sup>11</sup>, L. Paavolainen, M. D. Herrmann, M. Rohban, J. Hung, H. Hennig, J. Concannon, I. Smith, P. A. Clemons, S. Singh, P. Rees, P. Horvath, R. G. Linington, and A. E. Carpenter, *Nat. Methods* **14**, 849 (2017).
- [13] E. Cai, K. Marchuk, P. Beemiller, C. Beppler, M. G. Rubashkin, V. M. Weaver, A. Gérard, T.-L. Liu, B.-C. Chen, E. Betzig, F. Bartumeus, and M. F. Krummel, *Science* **356** (2017).
- [14] C. D. Paul, P. Mistriotis, and K. Konstantopoulos, *Nature Reviews Cancer* **17**, 131 (2017).
- [15] R. J. Petrie and K. M. Yamada, *Journal of Cell Science* **125**, 5917 (2012).
- [16] V. Sanz-Moreno, G. Gadea, J. Ahn, H. Paterson, P. Marra, S. Pinner, E. Sahai, and C. J. Marshall, *Cell* **135**, 510 (2008).
- [17] S. Wilkinson, H. F. Paterson, and C. J. Marshall, *Nat. Cell Biol.* **7**, 255 (2005).
- [18] V. Sanz-Moreno and C. J. Marshall, *Curr. Opin. Cell Biol.* **22**, 690 (2010).
- [19] R. J. Petrie and K. M. Yamada, *J. Cell Science* **125**, 5917 (2012).
- [20] M. Pavlaki and S. Zucker, *Cancer Metastasis Rev.* **22**, 177 (2003).
- [21] K. Wolf, I. Mazo, H. Leung, K. Engelke, U. H. von Andrian, E. I. Deryugina, A. Y. Strongin, E. Bröcker, and P. Friedl, *J. Cell Biol.* **160**, 267 (2003).
- [22] T. Yeung, P. C. Georges, L. A. Flanagan, B. Marg, M. Ortiz, M. Funaki, N. Zahir, W. Ming, V. Weaver, and P. A. Janmey, *Cell Motil. Cytoskeleton* **60**, 24 (2005).
- [23] K. Wolf, M. te Lindert, M. Krause, S. Alexander, J. te Riet, A. L. Willis, R. M. Hoffman, C. G. Figdor, S. J. Weiss, and P. Friedl, *J. Cell Biol.* **201**, 1069 (2013).
- [24] J. Sapudom, S. Rubner, S. Martin, T. Fischer, S. Riedel, C. T. Mierke, and T. Pompe, *Biomaterials* **52**, 367 (2015).
- [25] R. J. Petrie, H. M. Harlin, L. T. Korsak, , and K. M. Yamada, *J. Cell Biol.* **216**, 93 (2017).
- [26] C. Cortes and V. N. Vapnik, *Machine Learning* **20** (1995), 10.1007/BF00994018.
- [27] A. Ben-Hur, D. Horn, H. Siegelmann, and V. N. Vapnik, *Journal of Machine Learning Research* **2** (2001).
- [28] C. Szegedy, S. Ioffe, and V. Vanhoucke, *CoRR arXiv preprint* (2016).
- [29] L. van der Maaten, *Proceedings of the Twelfth International Conference on Artificial Intelligence & Statistics JMLR W&CP* **5**, 384 (2009).
- [30] J.-Y. Tinevez, U. Schulze, G. Salbreux, J. Roensch, J.-F. Joanny, and E. Paluch, *Proceedings of the National Academy of Sciences* **106**, 18581 (2009).
- [31] R. J. Petrie, N. Gavara, R. S. Chadwick, and K. M. Yamada, *J. Cell Biol.* **197**, 439 (2012).
- [32] M. R. Mejillano, S. Kojima, D. A. Applewhite, F. B. Gertler, T. M. Svitkina, and G. G. Borisy, *Cell* **118**, 363 (2004).
- [33] K. Yoshida and T. Soldat, *J. Cell Science* **119**, 3833 (2006).
- [34] J. B. Wyckoff, S. E. Pinner, S. Gschmeissner, J. S. Condeelis, and E. Sahai, *Curr. Biol.* **16**, 1515 (2006).
- [35] P. Wu, A. Giri, S. X. Sun, and D. Wirtz, *Proc. Natl. Acad. Sci.* **111**, 3949 (2014).
- [36] C. T. Mierke, B. Frey, M. Fellner, M. Herrmann, and B. Fabry, *Journal of Cell Science* **124**, 369 (2011).
- [37] A. A. Alobaidi and B. Sun, *Cancer Convergence* **1** (2017).
- [38] A. D. Doyle and K. M. Yamada, *Exp. Cell Res.* **343**, 60 (2016).
- [39] K. Jansen, P. Atherton, and C. Ballestrem, *Seminars in Cell and Developmental Biology* **71**, 75 (2017).
- [40] P. B. Gupta, C. M. Fillmore, G. Jiang, S. D. Shapira, K. Tao, C. Kuperwasser, and E. S. Lander, *Cell* **146**, 633 (2011).